Inorganic Chemistry

Article

pubs.acs.org/IC

Photocatalytic CO_2 Reduction to Formate Using a Mn(I) Molecular Catalyst in a Robust Metal–Organic Framework

Honghan Fei,[†] Matthew D. Sampson,[†] Yeob Lee, Clifford P. Kubiak,* and Seth M. Cohen*

Department of Chemistry and Biochemistry, University of California, San Diego, La Jolla, California 92093, United States

Supporting Information

ABSTRACT: A manganese bipyridine complex, Mn(bpydc)-$(CO)_3Br$ (bpydc = 5,5′-dicarboxylate-2,2′-bipyridine), has been incorporated into a highly robust Zr(IV)-based metal–organic framework (MOF) for use as a CO_2 reduction photocatalyst. In conjunction with $[Ru(dmb)_3]^{2+}$ (dmb = 4,4′-dimethyl-2,2′-bipyridine) as a photosensitizer and 1-benzyl-1,4-dihydronicotinamide (BNAH) as a sacrificial reductant, Mn-incorporated MOFs efficiently catalyze CO_2 reduction to formate in DMF/triethanolamine under visible-light irradiation. The photochemical performance of the Mn-incorporated MOF reached a turnover number of approximately 110 in 18 h, exceeding that of the homogeneous reference systems. The increased activity of the MOF-incorporated Mn catalyst is ascribed to the struts of the framework providing isolated active sites, which stabilize the catalyst and inhibit dimerization of the singly reduced Mn complex. The MOF catalyst largely retained its crystallinity throughout prolonged catalysis and was successfully reused over several catalytic runs.

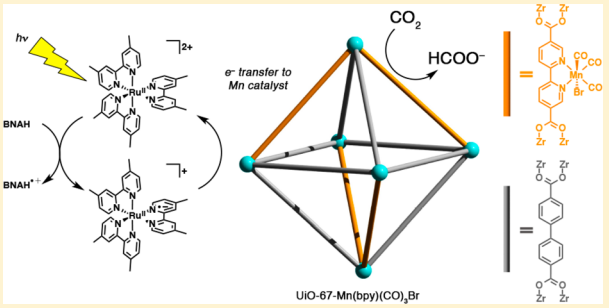

INTRODUCTION

With the global environmental demand and dwindling supply of fossil fuels, the chemical transformation of carbon dioxide (CO_2) into chemical fuels is of vital importance.[1−3] Because CO_2 is the most oxidized and stable form of carbon, overcoming this stability to reduce CO_2 to more useful chemicals is very energy intensive.[4] Mimicking a natural photosynthetic system using a photosensitizer, catalytic site, and sacrificial reducing agent is one viable approach to utilizing solar energy to activate and reduce CO_2.[5,6] Among artificial photosynthetic systems for CO_2 reduction, molecular complexes incorporating second and third row transition metals, such as Ru and Re, are considered to be benchmarks and generally exhibit the best performance.[7−10] However, the use of earth-abundant, first-row transition metal catalysts rather than precious metals is more attractive for an economically viable, sustainable technology.[11] Increasing the robustness of these artificial photocatalytic systems is important as well, as they often exhibit limited stability; thus, it is desirable to incorporate these systems into a heterogeneous matrix to achieve isolated active sites.[12,13]

Metal–organic frameworks (MOFs) have emerged as an intriguing class of crystalline and microporous materials with a vast array of topologies[14] and applications in gas absorption,[15,16] catalysis,[17,18] molecular separation,[19] chemical sensing,[20] and drug delivery.[21] The ability to design and tune the functional components of the organic linkers, along with inherently high porosity, allows MOFs to be a versatile platform for artificial photosynthesis.[22,23] A number of MOFs have been used as photocatalysts for both of the half reactions in water splitting (i.e., proton reduction[24−30] and water oxidation[31−33]). Site-isolation of molecular catalysts residing in MOFs allows for significantly enhanced stability of the catalytic complexes, thus improving long-term performance of these systems.[22]

The first example of photocatalytic MOFs for CO_2 reduction was demonstrated by Lin and co-workers, who doped *fac*-Re(bpydc)$(CO)_3Cl$ (bpydc = 5,5′-dicarboxylate-2,2′-bipyridine) into a UiO-67 (UiO = University of Oslo) framework to reduce CO_2 to carbon monoxide (CO) with a turnover number (TON) of 10.9 in 6 h.[31] In this system, Re site incorporation was limited (4.2 wt %), and the recovered MOFs were found to be inactive for additional photocatalytic cycles due to the detachment of the $Re(CO)_3$ moiety. Another strategy to achieve photocatalytic MOFs for CO_2 reduction involved the introduction of amino groups onto the organic dicarboxylate ligands of MIL-125(Ti) (MIL = Materials of the Institute Lavoisier) or UiO-66(Zr) solids.[34,35] Here, the functionalized MOFs reduced CO_2 to formate, and the photocatalytic performance was ascribed to visible light absorption by the amino-functionalized ligands and catalytically active Ti^{3+} or Zr^{3+} centers in the metal-oxo clusters. However, both of these examples showed low TONs (0.03 per catalytic site). Lee et al. employed postsynthetic exchange to introduce Ti into UiO-66(Zr) as well as a mixed-ligand strategy to achieve photocatalytic CO_2 reduction to formic acid with a TON ∼6.3.[36] Recently, Wang et al. reported efficient proton and CO_2 reduction using Co-ZIF-9 (ZIF = zeolitic imidazolate framework) in conjunction with $[Ru(bpy)_3]^{2+}$ (bpy = 2,2′-bipyridine) as a photosensitizer and TEOA as a sacrificial

Received: April 2, 2015
Published: July 2, 2015

DOI: 10.1021/acs.inorgchem.5b00752
Inorg. Chem. 2015, 54, 6821−6828

reductant, reaching a TON for CO as high as 89.6 within 30 min.[37] However, the mechanism for this high activity was not discussed, and the selectivity for CO_2 reduction against proton reduction was low (CO:H_2 ratio = ~1.4:1).

The earth-abundant Mn complex, *fac*-Mn(bpy)$(CO)_3$Br (the *fac*- label will be omitted throughout the remainder of the text for simplicity), has been shown to be an efficient electrocatalyst for CO_2 reduction to CO.[38−44] Recently, Takeda et al. reported on a photochemical system that incorporates this Mn catalyst for highly selective CO_2 reduction to formic acid.[45] The thermal instability of the $Mn(CO)_3$-moiety has proven difficult for incorporation of this Mn complex into MOFs via a conventional solvothermal manner.[31] Herein, we report the postsynthetic metalation of a robust Zr(IV)-based MOF with open bpy metal-chelating linkers to achieve isolated Mn(bpy)-$(CO)_3$Br moieties in the MOF. More importantly, in conjunction with $[Ru(dmb)_3]^{2+}$ (dmb = 4,4′-dimethyl-2,2′-bipyridine) as a redox photosenstizer and 1-benzyl-1,4-dihydronicotinamide (BNAH) as a sacrificial reducing agent, the resulting UiO-67-Mn(bpy)$(CO)_3$Br was found to be highly active and selective for the photocatalytic reduction of CO_2 to formate with a TON of 110 through 18 h of catalysis. UiO-67 materials exhibited catalytic activities exceeding those of the Mn(bpy)$(CO)_3$Br and Mn(bpydc)$(CO)_3$Br homogeneous analogues, as well as many precious-metal-based MOF photocatalysts. The UiO-67 matrix enhanced stability of the Mn active sites, allowing them to be reused up to three cycles.

EXPERIMENTAL SECTION

General Methods. Starting materials and solvents were purchased and used without further purification from commercial suppliers (Sigma-Aldrich, Alfa Aesar, EMD, TCI, Cambridge Isotope Laboratories, Inc., and others). DMF and TEOA were dried over 3 Å molecular sieves and stored under dry N_2 prior to use. Proton nuclear magnetic resonance spectra (^{1}H NMR) were recorded on a Varian FT-NMR spectrometer (400 MHz). Chemical shifts were quoted in parts per million (ppm) referenced to the appropriate solvent peak or 0 ppm for TMS. NMR spectra for photocatalysis product analysis were recorded on a Varian 300 MHz spectrometer at 298 K, and data were processed using Bruker TopSpin software. ESI−MS was performed using a ThermoFinnigan LCQ-DECA mass spectrometer, and the data were analyzed using the Xcalibur software suite. Inductively coupled plasma-optical emission spectroscopy (ICP-OES) was performed by Intertek USA, Inc. (Whitehouse, NJ). Mn(bpy)$(CO)_3$Br[46,47] and $[Ru(dmb)_3](PF_6)_2$ were prepared as previously reported.[48]

Synthesis of UiO-67-bpydc. $ZrCl_4$ (24.5 mg, 0.105 mmol), glacial acetic acid (189 mg, 3.15 mmol), biphenyl-4,4′-dicarboxylic acid (H_2bpdc, 13 mg, 0.053 mmol), and 2,2′-bipyridine-5,5′-dicarboxylic acid (H_2bpydc, 13 mg, 0.053 mmol) were placed in a scintillation vial with 4 mL of *N*,*N*′-dimethylformamide (DMF). The reagents were dispersed via sonication for ~10 min, followed by incubation at 120 °C for 24 h. After being cooled, the solids were isolated via centrifugation at 6000 rpm for 15 min using a fixed angle rotor, and the solvent was decanted. The solids were washed with DMF (2 × 10 mL), followed by soaking in methanol (MeOH) for 3 d, and the solution was exchanged with fresh MeOH (10 mL) every 24 h. After 3 d of soaking, the solids were collected via centrifugation and dried under vacuum. Yield: 33 mg (88% based on Zr).

Synthesis of UiO-67-Mn(bpy)$(CO)_3$Br. Bromopentacarbonylmanganese(I) ($Mn(CO)_5$Br, 14.1 mg, 0.05 mmol) was dissolved in 6 mL of diethyl ether (Et_2O). UiO-66-bpydc (30 mg, 0.042 mmol equiv of bpydc) was added to this Mn solution. The materials were dispersed via sonication for ~10 min, then incubated at room temperature for 24 h. After 24 h, the solids were isolated via centrifugation, and the red solids were washed profusely with Et_2O (3 × 10 mL), until the supernatant was colorless. The solids were left to soak in MeOH for 3 d, and the solution was exchanged with fresh MeOH (10 mL) every 24 h. After 3 d of soaking, the solids were collected via centrifugation and dried under vacuum (yield: ca. 99%). Because of the light-sensitive nature of Mn complex, the MOF incubation, washing, and drying steps were performed with minimal exposure to ambient light.

Synthesis of Mn(bpydc)$(CO)_3$Br. The synthesis of Mn(bpydc)-$(CO)_3$Br was performed with a slight modification to literature procedures.[49] $Mn(CO)_5$Br (200 mg, 2.17 mmol) was added to a N_2 sparged round-bottom flask containing 20 mL of Et_2O. The flask was covered in foil to shield it from ambient light. The H_2bpydc ligand (212 mg, 2.17 mmol) was added to the mixture, and the reaction was heated to reflux. After 3 h, the reaction mixture was allowed to cool to room temperature, and then the reaction flask was placed in a freezer for 2 h. After this time, a dark red solid was collected via vacuum filtration and dried under vacuum overnight. All spectroscopic characterization matched previous reports[49] and was consistent with the structure of the expected complex. Yield: 483 mg (48%).

Photocatalysis. Photochemical reactions were performed in a 36 mL quartz cell (NSG Precision Cell, Inc.; path length = 2 cm) equipped with a rubber septum (Supporting Information Figure S2). All experiments were performed in a DMF/TEOA solvent mixture (4:1 v/v, 20 mL total) containing 0.5 mM Mn catalyst, 0.5 mM $[Ru(dmb)_3](PF_6)_2$ as a photosensitizer, and 0.2 M BNAH as a sacrificial reductant. Each photochemical solution was sparged with dry N_2 for 5 min followed by dry CO_2 for 15 min prior to irradiation. N_2 and CO_2 gases were run through custom Drierite/molecular sieves (3 Å) drying columns before use. The photochemical cell was irradiated with a 470 nm LED (ThorLabs, Inc.), and the photochemical solutions were constantly stirred throughout each experiment. The light intensity was calculated to be 2.51×10^{-7} einstein/s, as determined by actinometry.[50] For recyclability studies, the photocatalytic solution was decanted, washed with acetone five times (decanted after each wash), and then dried under vacuum overnight to yield the postcatalysis UiO-67-Mn(bpy)$(CO)_3$Br solid. This retained solid was recycled for additional photocatalytic experiments.

Product Analysis from Photocatalysis. The headspace of the photochemical cell was analyzed for CO and H_2 products after each experiment. Gas analyses were performed using a 1 mL sample injection on a Hewlett-Packard 7890A Series gas chromatograph with two molsieve columns (30 m × 0.53 mm ID × 25 μm film). Each 1 mL injection was split between two columns, one with N_2 and one with He as the carrier gas, to quantify both CO and H_2 simultaneously in each run. Gas chromatography calibration curves were made by sampling known volumes of CO and H_2 gas. All photochemical solutions were analyzed for organic products via ^{1}H NMR after the following workup: a known concentration of ferrocene (typically ~5−8 mg), used as an internal standard, was added to a 5 mL aliquot of the irradiated solution, and the solution was sonicated for 10 min. A 0.8 mL aliquot of the resulting solution was added to a 2 mL volumetric flask containing 0.1 mmol of Verkade's base (2,8,9-triisobutyl-2,5,8,9-tetraaza-1-phosphabicyclo[3.3.3]undecane). The solution was diluted to 2 mL with CD_3CN, and the resulting solution was sonicated for 10 min. Three NMR samples were made from this solution, and each NMR sample was run for 128 scans on a Varian 300 MHz spectrometer at 298 K. The formate chemical shift (δ = ~8.50 ppm) was integrated against the ferrocene chemical shift (δ = ~4.14 ppm). Standard formate samples were prepared using the same procedure, starting with a nonirradiated, 20 mL sample of the following: a known concentration of formic acid, 0.5 mM Mn(bpy)-$(CO)_3$Br, 0.5 mM $[Ru(dmb)_3](PF_6)_2$, 0.2 M BNAH, 4:1 DMF:TEOA (v/v). Upon basic workup with Verkade's base and addition of a known concentration of ferrocene, ^{1}H NMR samples were used to create a calibration curve. The integration values for the formate chemical shift and the ferrocene chemical shift were used to calculate the [formate] in the NMR samples and, after back calculating, the [formate] in the photochemical solution. Blank NMR samples of nonirradiated, CO_2-saturated photochemical solutions showed no detectable production of formate, indicating that the Verkade's base does not produce formate in a solution of CO_2. Representative ^{1}H

DOI: 10.1021/acs.inorgchem.5b00752
Inorg. Chem. 2015, 54, 6821−6828

Scheme 1. Synthesis of UiO-67-Mn(bpy)(CO)$_3$Br

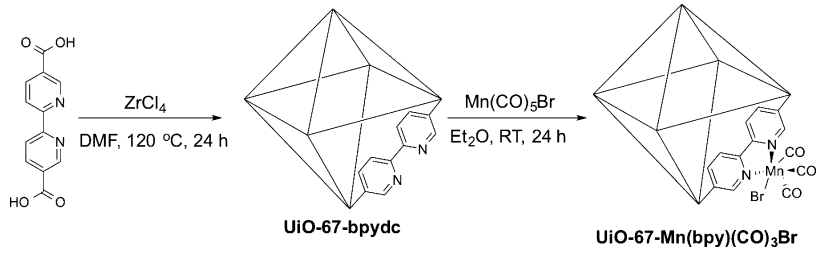

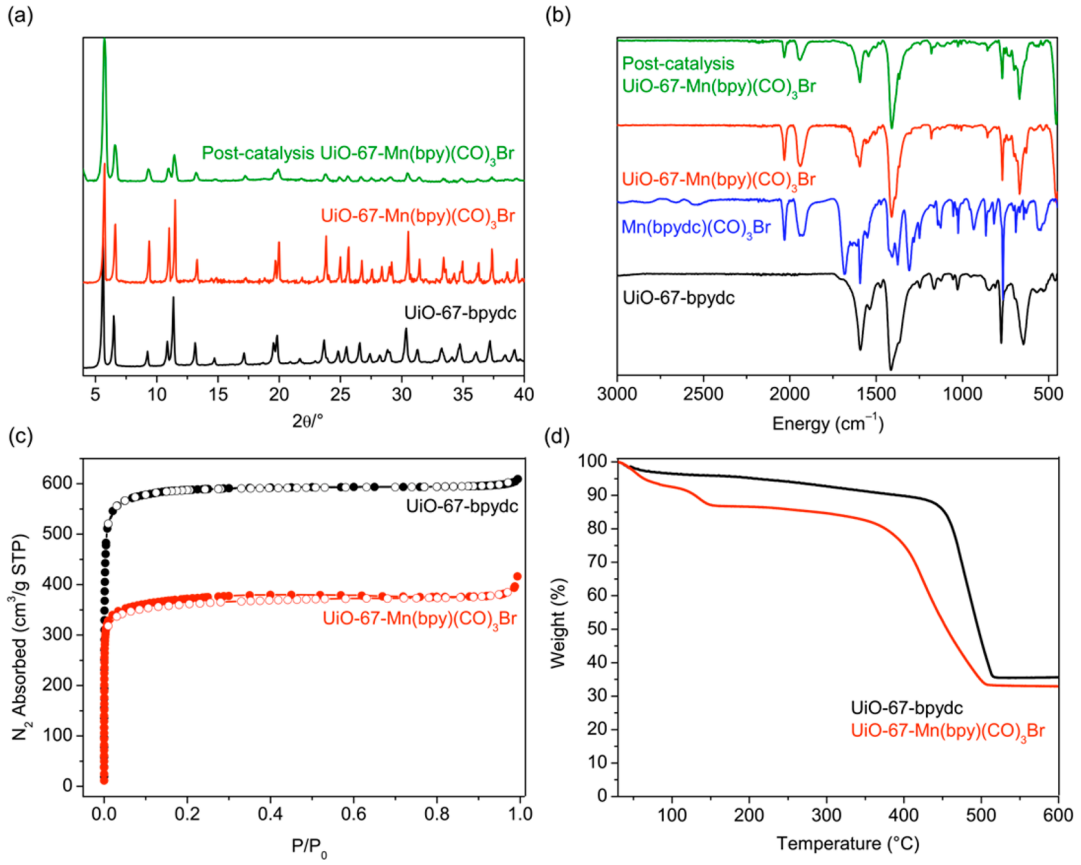

Figure 1. (a) PXRD of UiO-67-bpydc (black), UiO-67-Mn(bpy)(CO)$_3$Br (red), and UiO-67-Mn(bpy)(CO)$_3$Br after one 4 h photocatalysis experiment. (b) FTIR of UiO-67-bpydc (black), Mn(bpydc)(CO)$_3$Br (blue), UiO-67-Mn(bpy)(CO)$_3$Br (red), and UiO-67-Mn(bpy)(CO)$_3$Br (green) after 1 cycle of catalysis. (c) N_2 isotherm of UiO-67-bpydc (black) and UiO-67-Mn(bpy)(CO)$_3$Br (red). (d) TGA of UiO-67-bpydc (black) and UiO-67-Mn(bpy)(CO)$_3$Br (red).

NMR spectra for formate production are shown in Supporting Information Figure S3.

Powder X-ray Diffraction (PXRD) Analysis. ~20−30 mg of UiO-67 samples were dried under vacuum prior to PXRD analysis. PXRD data were collected at ambient temperature on a Bruker D8 Advance diffractometer at 40 kV, 40 mA for Cu Kα (λ = 1.5418 Å), with a scan speed of 1 s/step, a step size of 0.02° in 2θ, and a 2θ range of ~5−40° (sample dependent). The experimental backgrounds were corrected using the Jade 5.0 software package.

MOF Digestion and Analysis by ^{1}H NMR. ~10 mg of UiO-67 material was dried under vacuum and digested with sonication in 595 μL of DMSO-d_6 and 5 μL of 40% HF.

BET Surface Area Analysis. ~50 mg of UiO-67 sample was evacuated on a vacuum line overnight at room temperature. The sample was then transferred to a preweighed sample tube and degassed at 30 °C on a Micromeritics ASAP 2020 Adsorption Analyzer for a minimum of 12 h or until the outgas rate was <5 mmHg. The sample tube was reweighed to obtain a consistent mass for the degassed exchanged MOF. BET surface area (m^2/g) measurements were collected at 77 K by N_2 on a Micromeritics ASAP 2020 Adsorption Analyzer using the volumetric technique. The sample was then manually degassed on the analysis port at 30 °C for approximately 6 h. N_2 sorption isotherms were collected at 77 K.

Thermogravimetric Analysis. ~10−15 mg of UiO-67 sample was used for TGA measurements, after BET analysis (activated samples). Samples were analyzed under a stream of N_2 using a TA Instrument Q600 SDT running from room temperature to 800 °C with a scan rate of 5 °C/min.

Scanning Electron Microscopy-Energy Dispersed X-ray Spectroscopy. ~2−5 mg of activated UiO-67 materials was transferred to conductive carbon tape on a sample holder disk, and coated using a Cr-sputter coating for 8 s. A Philips XL ESEM instrument was used for acquiring images using a 10 kV energy source under vacuum. Oxford EDX and Inca software are attached to determine elemental mapping of particle surfaces at a working distance at 10 mm. ~19 000× magnification images were collected.

Fourier-Transformed Infrared (FTIR) Spectroscopy. ~5 mg of UiO-67 samples were dried under vacuum prior to FTIR analysis.

DOI: 10.1021/acs.inorgchem.5b00752
Inorg. Chem. 2015, 54, 6821−6828

FTIR data were collected at ambient temperature on a Bruker ALPHA FTIR spectrometer from 4000 and 450 cm^{-1}. The experimental backgrounds were corrected using OPUS software package.

RESULTS AND DISCUISSON

Synthesis of UiO-67-Mn(bpy)$(CO)_3$Br. The UiO series of MOFs were first discovered by Lillerud and co-workers and are constructed from $Zr_6O_4(OH)_4(CO_2)_{12}$ secondary building units and dicarboxylate bridging ligands.[51] The UiO-67 framework with open bpy chelating groups (UiO-67-bpydc) was synthesized using a direct solvothermal synthesis according to our previous report.[52] Heating a DMF solution containing a 1:1 molar ratio of H_2bpydc and 4,4′-biphenyldicarboxylic acid (H_2bpdc) with $ZrCl_4$ and acetic acid (as a modulator) at 120 °C for 24 h afforded highly crystalline UiO-67-bpydc containing 50 ± 4% bpydc (Scheme 1). After washing with MeOH and activation under dynamic vacuum, the high crystallinity and phase purity of UiO-67-bpydc were confirmed by powder X-ray diffraction (PXRD, Figure 1a). Field-emission scanning electron microscopy (FE-SEM) showed an octahedral morphology of the resultant materials with a crystal size ranging from 0.7−1 μm.

Attempts to directly include Mn(bpydc)$(CO)_3$Br into MOFs during solvothermal synthesis (100−120 °C) resulted in decomposition of the Mn complex, presumably due to the labile Mn−CO bonds. Taking advantage of mild postsynthetic modification (PSM) conditions,[53] we successfully introduced the targeted Mn complex onto the struts of UiO-67-bpydc framework. The activated UiO-67-bpydc was incubated in a diethyl ether (Et_2O) solution containing $Mn(CO)_5Br$ at room temperature for 24 h. The metalated material, UiO-67-Mn(bpy)$(CO)_3$Br, was isolated as a red microcrystalline powder, after washing thoroughly with fresh Et_2O and activation under vacuum. PXRD and FE-SEM confirmed the retention of the UiO-67 topology after metalation (Figure 1a, Supporting Information Figure S1). Dinitrogen (N_2) absorption/desorption isotherms (77 K) of UiO-67-bpydc and UiO-67-Mn(bpy)$(CO)_3$Br indicate a decrease in porosity upon metalation (Figure 1c), with Brunauer−Emmett−Teller (BET) surface areas determined to be 2340 ± 134 and 1430 ± 133 m^2/g for UiO-67-bpydc and UiO-67-Mn(bpy)$(CO)_3$Br, respectively. The lower BET surface area is consistent with the increased wt % and steric bulk of the Mn complexes residing in the metalated MOF, and the specific surface area is actually higher than that of other MOFs possessing metalated bpy sites.[54−56]

The degree of Mn(bpydc)$(CO)_3$Br functionalization was characterized by inductively coupled plasma-optical emission spectroscopy (ICP-OES), energy-dispersed X-ray spectroscopy (EDX), and thermogravimetric analysis (TGA). The ratio of heavy elements in UiO-67-Mn(bpy)$(CO)_3$Br was determined to be 1:0.376 (Zr:Mn) via ICP-OES and 1:0.39:0.37 (Zr:Mn:Br) via EDX, which suggests that ∼76% of bpy sites were metalated, achieving an overall formula of $Zr_6O_4(OH)_4(Mn(bpydc)(CO)_3Br)_{2.3}(bpydc)_{0.7}(bpdc)_3$. It was found that increasing the bpy functionalization to 75−100% for parent UiO-67-bpydc followed by Mn metalation did not significantly enhance the incorporation of Mn(bpy)$(CO)_3$Br moieties, perhaps due to steric hindrance by the Mn complexes in the MOF cavities. The TGA trace of UiO-67-Mn(bpy)-$(CO)_3$Br exhibited two decomposition steps at ∼70−150 and ∼370−500 °C, unlike pristine UiO-67-bpydc, which displayed only one major decomposition step at ∼450−500 °C (Figure 1d). The first decomposition step for UiO-67-Mn(bpy)-$(CO)_3$Br is likely due to thermal liberation of the carbonyl ligands bound to the Mn centers (obsd 7.2%, calcd 7.3%). The remaining organic ligands decompose at ∼370 °C, leading to mixed ZrO_2 and Mn_2O phases (obsd 33.4%, calcd 33.7%, percent weight residual mass). In addition, we employed Fourier-transform infrared spectroscopy (FTIR) to demonstrate the incorporation of the targeted Mn(bpy)$(CO)_3$Br complex into the MOF. FTIR of UiO-67-Mn(bpy)$(CO)_3$Br exhibited two prominent CO stretching frequencies at 2031 and 1940 cm^{-1}, while no such CO bands were observed between 2200−1800 cm^{-1} for the parent UiO-67-bpydc material (Figure 1b). Moreover, the position and relative intensity of these characteristic CO stretching frequencies was identical to those of the free Mn(bpydc)$(CO)_3$Br complex, suggesting successful formation of the targeted catalytic site on the strut of the MOFs. Indeed, the color change (colorless to red) during metalation is due to the coordination of Mn(I) to the nitrogen atoms of the bpydc ligand and is ascribed to the metal-to-ligand (Mn^I → bipyridine π^*) charge transfer (MLCT) band.

Photocatalytic CO_2 Reduction. Having observed successful incorporation of the Mn complex into a robust MOF, we explored the efficiency of this material as a catalyst in photochemical CO_2 reduction. In tandem with $[Ru(dmb)_3]^{2+}$ (0.5 mM) as a redox photosensitizer and BNAH (0.2 M) as a sacrificial reductant, visible light irradiation (470 nm) of a mixed solution of DMF and TEOA (4:1 v/v) containing UiO-67-Mn(bpy)$(CO)_3$Br (0.5 mM Mn sites) and saturated with CO_2 afforded highly selective production (∼96%) of formate (see a simplified scheme of the photocatalysis apparatus in the Supporting Information, Figure S2). UiO-67-Mn(bpy)-$(CO)_3$Br-catalyzed formate production reached TONs of 50 ± 7.8 and 110 ± 13 over 4 and 18 h, respectively (Figure 2 and Table 1). Production of formate was determined by ^{1}H NMR spectroscopy after a basic workup and comparison with both an internal standard (ferrocene) and formate standard solutions

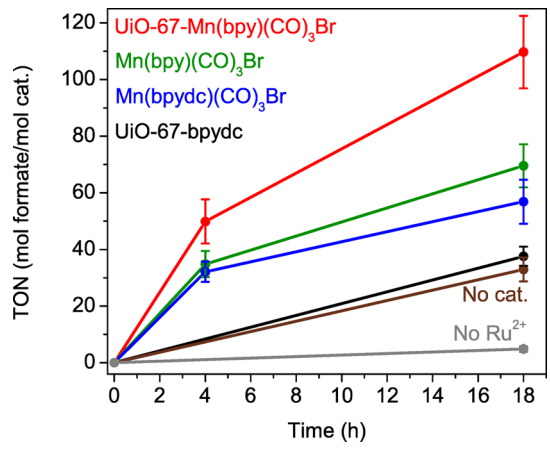

Figure 2. Plot of formate turnover number (TON, mol of formate/mol of catalyst) during photocatalysis experiments for the following systems: UiO-67-Mn(bpy)$(CO)_3$Br (red), Mn(bpy)$(CO)_3$Br (green), Mn(bpydc)$(CO)_3$Br (blue), UiO-67-bpydc (black), no added Mn complex or MOF (only Ru^{2+}, brown), and UiO-67-Mn(bpy)$(CO)_3$Br without added Ru^{2+} (gray). All photocatalytic experiments were performed in a DMF/TEOA (4:1 v/v, 20 mL total) solution with 0.5 mM catalyst, 0.5 mM $[Ru(dmb)_3]^{2+}$, 0.2 M BNAH with CO_2 saturation, and irradiated with 470 nm light (unless otherwise noted).

DOI: 10.1021/acs.inorgchem.5b00752
Inorg. Chem. 2015, 54, 6821−6828

Table 1. Turnover Numbers (TONs) for Formate ($HCOO^-$), CO, and H_2 from Photocatalytic Experiments[a]

entry	system	irradiation time (h)	$HCOO^-$ TON	$HCOO^-$ Φ	CO TON	H_2 TON
1	UiO-67-Mn(bpy)$(CO)_3$Br[b]	4	50 ± 7.8	13.8%	1.5 ± 2.0	0.41 ± 0.54
2	UiO-67-Mn(bpy)$(CO)_3$Br[b]	18	110 ± 13	6.74%	4.5 ± 0.73	1.0 ± 0.11
3	UiO-67-Mn(bpy)$(CO)_3$Br (reused 1)[c]	4	24 ± 6.4	6.64%	0.73	0.46
4	UiO-67-Mn(bpy)$(CO)_3$Br (reused 2)[c]	4	19 ± 2.3	5.25%	0.64	0.48
5	UiO-67-Mn(bpy)$(CO)_3$Br (reused 3)[c]	4	17 ± 2.0	4.70%	0.51	0.49
6	Mn(bpy)$(CO)_3$Br	4	35 ± 4.6	9.64%	2.1	0.01
7	Mn(bpy)$(CO)_3$Br	18	70 ± 7.6	4.27%	5.1	0.14
8	Mn(bpydc)$(CO)_3$Br	4	32 ± 3.6	8.89%	2.3	0.03
9	Mn(bpydc)$(CO)_3$Br	18	57 ± 7.8	3.49%	5.2	0.06
10	UiO-67-bpydc	18	38 ± 3.4	2.31%	0.40	0.42
11	Only $[Ru(dmb)_3]^{2+}$[d]	18	33 ± 4.2	2.02%	0.30	0.29
12	UiO-67-Mn(bpy)$(CO)_3$Br, no $[Ru(dmb)_3]^{2+}$[e]	18	4.9 ± 1.0	0.30%	0.02	0.0
13	UiO-67-Mn(bpy)$(CO)_3$Br, under N_2[f]	18	2.1 ± 1.4	0.13%	1.0	8.3
14	UiO-67 and Mn(bpy)$(CO)_3$Br[g]	18	73 ± 3.6	4.46%	4.3	0.02

[a]All photocatalytic experiments were performed in a DMF/TEOA (4:1 v/v, 20 mL total) solution with 0.5 mM catalyst, 0.5 mM $[Ru(dmb)_3]^{2+}$, and 0.2 M BNAH with CO_2 saturation (unless otherwise noted). All experiments were irradiated with 470 nm monochromatic light (intensity = 2.51×10^{-7} einstein s^{-1}). [b]Experiments with UiO-67-Mn(bpy)$(CO)_3$Br were performed at [Mn] = 0.5 mM using the formula $Zr_6O_4(OH)_4$(Mn(bpydc)-$(CO)_3Br)_{2.3}$(bpydc)$_{0.7}$(bpdc)$_3$. [c]The MOF solids were recovered from the previous 4 h photocatalysis experiment by decanting the solution, washing with acetone, and drying under vacuum before being reused in a new catalytic run. [d]Experiment did not contain any Mn catalyst or UiO-67 MOF. [e]Experiment did not contain any $[Ru(dmb)_3]^{2+}$ photosensitizer. [f]Experiment was performed under N_2 atmosphere. [g]Experiment performed with 0.5 mM UiO-67 and 0.5 mM Mn(bpy)$(CO)_3$Br.

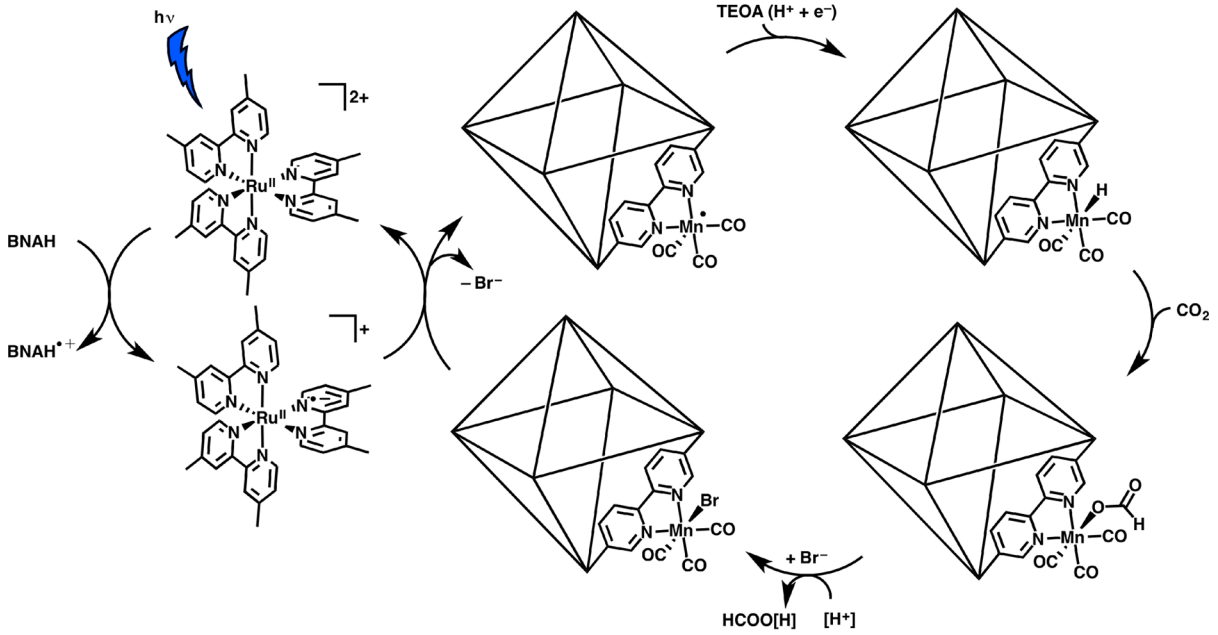

Figure 3. Proposed mechanism for the formation of formate from the photocatalytic reaction with UiO-67-Mn(bpy)$(CO)_3$Br.

(Supporting Information Figure S3). With a light intensity of 2.51×10^{-7} einstein s^{-1}, the Mn-functionalized MOF produced formate with a quantum yield ($\Phi_{formate}$) of 13.8% over the course of 4 h. Additionally, these photocatalysis experiments produced low yields of CO and dihydrogen (H_2), as determined by gas chromatography (CO TON = 1.5 and 4.5; H_2 TON = 0.41 and 1.0 for 4 and 18 h, respectively). To directly compare the CO_2 reduction ability of UiO-67-Mn(bpy)$(CO)_3$Br to the homogeneous catalytic system, we synthesized both Mn(bpy)$(CO)_3$Br and Mn(bpydc)$(CO)_3$Br and studied these complexes as photosensitized catalysts. UiO-67-Mn(bpy)$(CO)_3$Br out-performed each homogeneous Mn complex in formate production over 4 and 18 h experiments (Figure 2, Table 1). Specifically, Mn(bpy)$(CO)_3$Br and Mn(bpydc)$(CO)_3$Br reached TONs for formate of 70 ± 7.6 and 57 ± 7.8 after 18 h (Table 1, entries 7, 9). UiO-67-Mn(bpy)$(CO)_3$Br out-performed a mixture of the homogeneous Mn(bpy)$(CO)_3$Br complex in combination with UiO-67 (Table 1, entry 14). It is important to note that, although photocatalytic reactions were run for a total of 18 h, this likely does not represent the lifetime of the catalyst under these photocatalytic conditions (see details on recyclability studies below). These 18 h photocatalytic experiments are reported to demonstrate the maximum TONs for each catalyst in one run.

The framework of UiO-67-Mn(bpy)$(CO)_3$Br clearly aids in catalysis, likely by both stabilizing the Mn$(CO)_3$ moiety and inhibiting dimerization in the singly reduced Mn complex (see below). Additionally, UiO-67 could serve as a reservoir of CO_2

DOI: 10.1021/acs.inorgchem.5b00752
Inorg. Chem. 2015, 54, 6821−6828

for supplying CO_2 to the Mn active sites. UiO-67 displays a CO_2 adsorption capacity of ~25 cc/g at room temperature and 1 bar of CO_2 (~2.4 CO_2/UiO-67 unit cell).[57,58] Hence, UiO-67 may sequester CO_2 at the Mn active sites when compared to the homogeneous Mn complexes, which have no ability to sequester or concentrate CO_2. However, in the presence of solvents, it is unlikely that UiO-67 functions as an additional CO_2 reservoir to aid in catalysis. The photocatalytic ability of UiO-67-Mn(bpy)$(CO)_3$Br compares very favorably with other MOFs that have been investigated for photocatalytic CO_2 reduction (Supporting Information Table S1).

In Figure 3, we present a proposed mechanism for the photocatalytic reaction. In these reactions, BNAH serves as the sacrificial reductant, reducing the excited Ru(II) photosensitizer and initiating the photocatalytic reaction. The reduced photosensitizer transfers an electron to the Mn catalyst, forming a Mn(0) complex that can then engage in catalysis. The large pores of UiO-67 (pore diameter = 1−2.3 nm)[57,59] are sufficient to allow electron transfer between the Ru(II) photosensitizer (longest molecular dimension = ~1.5 nm) and the Mn complex within the MOF, as the Ru(II) photosensitizer is capable of accessing the interior of UiO-67. To further support this claim, soaking UiO-67 in a solution of the Ru(II) photosensitizer resulted in a color change to the MOF (persisting after multiple washes with acetone), suggestive of encapsulation of the Ru(II) complex within the MOF. TEOA likely facilitates the reaction by donating a sacrificial proton and electron (i.e., a hydrogen atom) during catalysis via a Hofmann-type degradation process (see our proposed mechanism in Figure 3).[60] It is unknown whether or not TEOA coordinates to the Mn center during this process; however, previous studies with Re bipyridine photocatalysts have shown that CO_2 can bind to the metal center with the aid of TEOA, forming an O-bound Re−$OC(O)OCH_2CH_2NR_2$ complex.[61] Additionally, these studies have shown that the aforementioned Re−OC(O)R complex can convert into a Re−OC(O)H complex under similar photocatalytic conditions (i.e., TEOA donates a hydrogen atom to the Re complex). In any case, we suggest TEOA donating one proton and one electron to the catalytic reaction, forming a Mn(I)−H complex. CO_2 can insert into the Mn−H bond, forming a Mn(I)−OC(O)H complex. Formate (or formic acid after further protonation) can then dissociate from the Mn center regenerating the starting Mn(I) complex. These conclusions are drawn from a large body of previous work published by others on photosensitized catalysis driven by sacrificial reducing agents.[62−67]

It is important to note that photocatalysis experiments without UiO-67-Mn(bpy)$(CO)_3$Br or a homogeneous Mn catalyst (i.e., with only the Ru^{2+} photosensitizer and BNAH) still catalyzed the production of formate, with a TON of 33 ± 4.2 over 18 h (Table 1, entry 11). Photocatalysis experiments with unmetalated UiO-67-bpydc showed similar yields of formate, with a TON of 38 ± 3.4 over 18 h (Table 1, entry 10). These TONs without Mn complex are not surprising given that in 1985 Hawecker et al. reported that $[Ru(bpy)_3]^{2+}$ is a homogeneous catalyst for the photochemical reduction of CO_2 to formate.[68] In the original report of the photocatalytic ability of Mn(bpy)$(CO)_3$Br by Takeda et al. in 2014, the authors report slightly lower TONs for formate by only the Ru^{2+} photosensitizer (TON = 25 after 12 h).[45] Although the $[Ru(dmb)_3]^{2+}$ photosensitizer also serves as a catalyst for CO_2 reduction, it is clear that the Mn complex enhances CO_2 reduction to formate by at least a factor of ~2 in the homogeneous system and a factor of ~3 in the heterogeneous UiO-67-Mn(bpy)$(CO)_3$Br system. Photocatalysis experiments under dinitrogen (N_2) atmosphere or without added Ru^{2+} photosensitizer resulted in minimal formation of formate over 18 h (Table 1, entries 12,13).

With respect to the mechanism of photocatalysis, upon a photoinduced one-electron reduction of Mn(bpy)$(CO)_3$Br, the Mn−Mn dimer, $[Mn(bpy)(CO)_3]_2$, is rapidly formed.[38−40] Bourrez et al. have identified this Mn−Mn dimer as an active catalyst for electrocatalytic CO_2 reduction to CO.[44] During visible-light irradiation, the Ru photosensitizer is selectively photoexcited, and the excited state of $[Ru(dmb)_3]^{2+}$ is reductively quenched by BNAH to give $[Ru(dmb)_2(dmb^{\bullet-})]^{+}$. This reduced Ru complex has sufficient reducing power to transfer one electron to Mn(bpy)$(CO)_3$Br,[45] which immediately forms the Mn−Mn dimer upon reduction. Takeda et al. suggested that the active catalyst for photochemical CO_2 reduction was a monomeric Mn radical species, citing evidence from UV−vis, FTIR, and ^{1}H NMR experiments.[45] Additionally, photoexcitation of similar Mn−Mn dimers, such as $[(CO)_2(bpy)Mn-Mn(CO)_5]$, efficiently induced cleavage of the Mn−Mn bond to the corresponding Mn radical species.[69−71] Indeed, if a monomeric Mn radical species is the active catalyst for photochemical CO_2 reduction to formate, then the framework of UiO-67-Mn(bpy)$(CO)_3$Br sufficiently eliminates dimerization prior to formation of the active catalyst, which as a result significantly enhances the efficiency for photochemical CO_2 reduction. Because the Mn sites in UiO-67-Mn(bpy)$(CO)_3$Br cannot dimerize upon one-electron reduction and UiO-67-Mn(bpy)$(CO)_3$Br operates as an efficient photocatalyst, the active catalyst for CO_2 reduction to formate is likely a monomeric species.

To further gauge the ability of the external UiO-67 framework to enhance the stability of the Mn catalyst, catalyst recyclability studies were performed using UiO-67-Mn(bpy)-$(CO)_3$Br (Table 1, entries 3−5). In these studies, the MOF was recovered by decanting off the reaction mixture, washing the MOF with acetone, and drying the MOF under vacuum before being used in a new photocatalytic experiment. Significant TONs for formate were detected after three consecutive 4 h photocatalytic runs. More specifically, UiO-67-Mn(bpy)-$(CO)_3$Br retained ~48%, ~38%, and ~34% activity after one, two, and three 4 h experiments, respectively. Postcatalysis FTIR of MOFs after one catalytic cycle indicates a significant loss of the $Mn(CO)_3$ moiety residing in the framework, with only ~37% of $Mn(CO)_3$ remaining (Figure 1b). Postcatalysis PXRD indicates that crystallinity is largely retained after the first 4 h run (Figure 1a). The persistance of some Mn active sites residing in UiO-67-Mn(bpy)$(CO)_3$Br was also confirmed using ICP-OES, with the atomic ratio of Zr:Mn decreasing only from 1:0.376 to 1:0.361 after one 4 h experiment. Therefore, the reduced photochemical performance over a few catalytic cycles is likely due to loss of the $Mn(CO)_3$ moiety in the framework, resulting from both prolonged irradiation by visible light and prolonged exposure to the alkaline photochemical solution. This is also confirmed by the postcatalysis characterization of UiO-67-Mn(bpy)$(CO)_3$Br after four catalytic cycles. After these four cycles, a large portion of the MOF solid was degraded and dissolved in the alkaline photocatalytic solution. At this time, FTIR indicated the negligible survival of the $Mn(CO)_3$ moiety in the MOF framework (Supporting Information Figure S4), and ICP-OES gave a Zr:Mn ratio of

DOI: 10.1021/acs.inorgchem.5b00752
Inorg. Chem. 2015, 54, 6821−6828

1:0.324. These data indicate that the main sources for loss of catalytic activity for each consecutive photocatalytic cycle are both the loss of CO ligands from the Mn catalytic sites and the degradation of the MOF framework.

CONCLUSION

We employed PSM as a mild functionalization technique to incorporate an earth-abundant, but thermally unstable, molecular photocatalyst for CO_2 reduction into a robust MOF platform. The resulting UiO-67-Mn(bpy)$(CO)_3$Br combines the efficient photochemical performance of Mn active sites with the enhanced stability of the solid-state MOF host. This Mn-incorporated MOF functions as a highly efficient CO_2 reduction catalyst under visible-light irradiation. The overall TON and selectivity of CO_2 reduction to formate for this Mn-incorporated MOF exceed not only the homogeneous reference systems, but also many precious-metal-based MOF photocatalysts (Supporting Information Table S1). Using UiO-67-Mn(bpy)$(CO)_3$Br, TONs for formate reached 50 and 110 over 4 and 18 h, respectively, displaying a selectivity of 96% over 4 h. The robust nature of the Zr(IV)-based MOF and isolation of the molecular catalytic sites inhibit dimerization of the singly reduced Mn catalyst, enabling some (albeit, low) degree of reusability over three catalytic cycles. Because of the low degree of recyclability achieved in this Mn-functionalized MOF, future studies will be focused on exploring other, more stable MOFs and other porous materials as supports for these Mn catalysts. Additionally, future studies will include varying photocatalytic conditions to increase the stability of the Mn–MOF construct and investigating the use of different photosensitizers to isolate the catalytic activity of only the Mn catalytic sites. These findings open new opportunities for artificial photosynthesis by immobilizing and protecting molecular catalysts in MOFs, thus enhancing their performance for photocatalysis.

ASSOCIATED CONTENT

Supporting Information

Additional characterization. The Supporting Information is available free of charge on the ACS Publications website at DOI: 10.1021/acs.inorgchem.5b00752.

AUTHOR INFORMATION

Corresponding Authors

*E-mail: ckubiak@ucsd.edu.
*E-mail: scohen@ucsd.edu.

Author Contributions

†H.F. and M.D.S. contributed equally.

Notes

The authors declare no competing financial interest.

ACKNOWLEDGMENTS

This work was supported by a grant from the National Science Foundation, Division of Materials Research (DMR-1262226), and by a grant from the Air Force Office of Scientific Research, MURI program (FA9550-10-1-0572).

REFERENCES

(1) Barber, J. *Chem. Soc. Rev.* **2009**, *38*, 185.
(2) Aresta, M. *Carbon Dioxide as a Chemical Feedstock*; Wiley-VCH: Weinheim, 2010.
(3) Chueh, W. C.; Falter, C.; Abbott, M.; Scipio, D.; Furler, P.; Haile, S. M.; Steinfeld, A. *Science* **2010**, *330*, 1797.
(4) Mikkelsen, M.; Jorgensen, M.; Krebs, F. C. *Energy Environ. Sci.* **2010**, *3*, 43.
(5) Devens, G.; Moore, T. A.; Moore, A. L. *Acc. Chem. Res.* **2009**, *42*, 1890.
(6) Morris, A. J.; Meyer, G. J.; Fujita, E. *Acc. Chem. Res.* **2009**, *42*, 1983.
(7) Morimoto, T.; Nishiura, C.; Tanaka, M.; Rohacova, J.; Nakagawa, Y.; Funada, Y.; Koike, K.; Yamamoto, Y.; Shishido, S.; Kojima, T.; Saeki, T.; Ozeki, T.; Ishitani, O. *J. Am. Chem. Soc.* **2013**, *135*, 13266.
(8) Tanaka, K.; Ooyama, D. *Coord. Chem. Rev.* **2002**, *226*, 211.
(9) Benson, E. E.; Kubiak, C. P.; Sathrum, A. J.; Smieja, J. M. *Chem. Soc. Rev.* **2009**, *38*, 89.
(10) Sato, S.; Morikawa, T.; Saeki, S.; Kajino, T.; Motohiro, T. *Angew. Chem., Int. Ed.* **2010**, *49*, 5101.
(11) Thoi, V. S.; Chang, C. J. *Chem. Commun.* **2011**, *47*, 6578.
(12) Kudo, A.; Miseki, Y. *Chem. Soc. Rev.* **2009**, *38*, 253.
(13) Qu, Y.; Duan, X. *Chem. Soc. Rev.* **2013**, *42*, 2568.
(14) Eddaoudi, M.; Sava, D. F.; Eubank, J. F.; Adil, K.; Guillerm, V. *Chem. Soc. Rev.* **2015**, *44*, 228.
(15) Sumida, K.; Rogow, D. L.; Mason, J. A.; McDonald, T. M.; Bloch, E. D.; Herm, Z. R.; Bae, T.-H.; Long, J. R. *Chem. Rev.* **2012**, *112*, 724.
(16) Suh, M. P.; Park, K. S.; Prasad, T. K.; Lim, D. *Chem. Rev.* **2012**, *112*, 782.
(17) Liu, J.; Chen, L.; Cui, H.; Zhang, J.; Zhang, L.; Su, C.-Y. *Chem. Soc. Rev.* **2014**, *43*, 6011.
(18) Yoon, M.; Srirambalaji, R.; Kim, K. *Chem. Rev.* **2012**, *112*, 1196.
(19) Van de Voorde, B.; Bueken, B.; Denayer, J.; De Vos, D. *Chem. Soc. Rev.* **2014**, *43*, 5766.
(20) Kreno, L. E.; Leong, K.; Farha, O. K.; Allendorf, M.; Van Duyne, R. P.; Hupp, J. T. *Chem. Rev.* **2012**, *112*, 1105.
(21) Horcajada, P.; Gref, R.; Baati, T.; Allan, P. K.; Maurin, G.; Couvreur, P.; Ferey, G.; Morris, R. E.; Serre, C. *Chem. Rev.* **2012**, *112*, 1232.
(22) Zhang, T.; Lin, W. *Chem. Soc. Rev.* **2014**, *43*, 5982.
(23) Wang, J.-L.; Wang, C.; Lin, W. *ACS Catal.* **2012**, *2*, 2630.
(24) Kataoka, Y.; Sato, K.; Miyazaki, Y.; Masuda, K.; Tanaka, H.; Naito, S.; Mori, W. *Energy Environ. Sci.* **2009**, *2*, 397.
(25) Fateeva, A.; Chater, P. A.; Ireland, C. P.; Tahir, A. A.; Khimyak, Y. Z.; Wiper, P. V.; Darwent, J. R.; Rosseinsky, M. J. *Angew. Chem., Int. Ed.* **2012**, *51*, 7440.
(26) Pullen, S.; Fei, H.; Orthaber, A.; Cohen, S. M.; Ott, S. *J. Am. Chem. Soc.* **2013**, *135*, 16997.
(27) Wang, C.; deKrafft, K. E.; Lin, W. *J. Am. Chem. Soc.* **2012**, *134*, 7211.
(28) Sasan, K.; Lin, Q.; Mao, C.; Feng, P. *Chem. Commun.* **2014**, *50*, 10390.
(29) Nasalevich, M. A.; Becker, R.; Ramos-Fernandez, E. V.; Castellanos, S.; Veber, S. L.; Fedin, M. V.; Kapteijn, F.; Reek, J. N. H.; van de Vlugt, J. I.; Gascon, J. *Energy Environ. Sci.* **2015**, *8*, 364.
(30) Zhou, T.; Du, Y.; Borgna, A.; Hong, J.; Wang, Y.; Han, J.; Zhang, W.; Xu, R. *Energy Environ. Sci.* **2013**, *6*, 3229.
(31) Wang, C.; Xie, Z.; deKrafft, K. E.; Lin, W. *J. Am. Chem. Soc.* **2011**, *133*, 13445.
(32) Wang, C.; Wang, J.-L.; Lin, W. *J. Am. Chem. Soc.* **2012**, *134*, 19895.
(33) Nepal, B.; Das, S. *Angew. Chem., Int. Ed.* **2013**, *52*, 7224.
(34) Fu, Y.; Sun, D.; Chen, Y.; Huang, R.; Ding, Z.; Fu, X.; Li, Z. *Angew. Chem., Int. Ed.* **2012**, *51*, 3364.
(35) Sun, D.; Fu, Y.; Liu, W.; Ye, L.; Wang, D.; Yang, L.; Fu, X.; Li, Z. *Chem.—Eur. J.* **2013**, *19*, 14279.
(36) Lee, Y.; Kim, S.; Kang, J. K.; Cohen, S. M. *Chem. Commun.* **2015**, DOI: 10.1039/c5cc00686d.
(37) Wang, S.; Yao, W.; Lin, J.; Ding, Z.; Wang, X. *Angew. Chem., Int. Ed.* **2014**, *53*, 1034.
(38) Sampson, M. D.; Nguyen, A. D.; Grice, K. A.; Moore, C. E.; Rheingold, A. L.; Kubiak, C. P. *J. Am. Chem. Soc.* **2014**, *136*, 5460.

DOI: 10.1021/acs.inorgchem.5b00752
Inorg. Chem. 2015, 54, 6821–6828

(39) Smieja, J. M.; Sampson, M. D.; Grice, K. A.; Benson, E. E.; Froehlich, J. D.; Kubiak, C. P. *Inorg. Chem.* **2013**, *52*, 2484.
(40) Bourrez, M.; Molton, F.; Chardon-Noblat, S.; Deronzier, A. *Angew. Chem., Int. Ed.* **2011**, *123*, 10077.
(41) Grice, K. A.; Kubiak, C. P. In *Advances in Inorganic Chemistry*; Michele, A., Rudi van, E., Eds.; Academic Press: New York, 2014; Vol. *66*, p 163.
(42) Franco, F.; Cometto, C.; Ferrero Vallana, F.; Sordello, F.; Priola, E.; Minero, C.; Nervi, C.; Gobetto, R. *Chem. Commun.* **2014**, *50*, 14670.
(43) Walsh, J. J.; Neri, G.; Smith, C. L.; Cowan, A. J. *Chem. Commun.* **2014**, *50*, 12698.
(44) Bourrez, M.; Orio, M.; Molton, F.; Vezin, H.; Duboc, C.; Deronzier, A.; Chardon-Noblat, S. *Angew. Chem., Int. Ed.* **2014**, *53*, 240.
(45) Takeda, H.; Koizumi, H.; Okamoto, K.; Ishitani, O. *Chem. Commun.* **2014**, *50*, 1491.
(46) Bourrez, M.; Molton, F.; Chardon-Noblat, S.; Deronzier, A. *Angew. Chem., Int. Ed.* **2011**, *50*, 9903.
(47) Staal, L. H.; Oskam, A.; Vrieze, K. *J. Organomet. Chem.* **1979**, *170*, 235.
(48) Sullivan, B. P.; Salmon, D. J.; Meyer, T. J. *Inorg. Chem.* **1978**, *17*, 3334.
(49) Blake, A. J.; Champness, N. R.; Easun, T. L.; Allan, D. R.; Nowell, H.; George, M. W.; Jia, J.; Sun, X.-Z. *Nat. Chem.* **2010**, *2*, 688.
(50) Hatchard, C. G.; Parker, C. A. *Proc. R. Soc. London, Ser. A* **1956**, *235*, 518.
(51) Cavka, J. H.; Jakobsen, S.; Olsbye, U.; Guillou, N.; Lamberti, C.; Bordiga, S.; Lillerud, K. P. *J. Am. Chem. Soc.* **2008**, *130*, 13850.
(52) Fei, H.; Cohen, S. M. *Chem. Commun.* **2014**, *50*, 4810.
(53) Cohen, S. M. *Chem. Rev.* **2012**, *112*, 970.
(54) Bloch, E. D.; Britt, D.; Lee, C.; Doonan, C. J.; Uribe-Romo, F. J.; Furukwa, H.; Long, J. R.; Yaghi, O. M. *J. Am. Chem. Soc.* **2010**, *132*, 14382.
(55) Carson, F.; Agrawal, S.; Gustafsson, M.; Bartoszewicz, A.; Moraga, F.; Zou, X.; Martin-Matute, B. *Chem.—Eur. J.* **2012**, *18*, 15337.
(56) Manna, K.; Zhang, T.; Lin, W. *J. Am. Chem. Soc.* **2014**, *136*, 6566.
(57) Wang, B.; Huang, H.; Lv, X.-L.; Xie, Y.; Li, M.; Li, J.-R. *Inorg. Chem.* **2014**, *53*, 9254.
(58) Ko, N.; Hong, J.; Sung, S.; Cordova, K. E.; Park, H. J.; Yang, J. K.; Kim, J. *Dalton Trans.* **2015**, *44*, 2047.
(59) Katz, M. J.; Brown, Z. J.; Colon, Y. J.; Siu, P. W.; Scheidt, K. A.; Snurr, R. Q.; Hupp, J. T.; Farha, O. K. *Chem. Commun.* **2013**, *49*, 9449.
(60) Georgopoulos, M.; Hoffman, M. Z. *J. Phys. Chem.* **1991**, *95*, 7717.
(61) Morimoto, T.; Nakajima, T.; Sawa, S.; Nakanishi, R.; Imori, D.; Ishitani, O. *J. Am. Chem. Soc.* **2013**, *135*, 16825.
(62) Hawecker, J.; Lehn, J.-M.; Ziessel, R. *J. Chem. Soc., Chem. Commun.* **1983**, 536.
(63) Hori, H.; Takano, Y.; Koike, K.; Sasaki, Y. *Inorg. Chem. Commun.* **2003**, *6*, 300.
(64) Shinozaki, K.; Hayashi, Y.; Brunschwig, B.; Fujita, E. *Res. Chem. Intermed.* **2007**, *33*, 27.
(65) Fujita, E.; Hayashi, Y.; Kita, S.; Brunschwig, B. S. In *Studies in Surface Science and Catalysis*; Sang-Eon Park, J.-S. C., Kyu-Wan, L., Eds.; Elsevier: New York, 2004; Vol. *153*, p 271.
(66) Agarwal, J.; Johnson, R. P.; Li, G. *J. Phys. Chem. A* **2011**, *115*, 2877.
(67) Hayashi, Y.; Kita, S.; Brunschwig, B. S.; Fujita, E. *J. Am. Chem. Soc.* **2003**, *125*, 11976.
(68) Hawecker, J.; Lehn, J.-M.; Ziessel, R. *Chem. Commun.* **1985**, 56.
(69) Meyer, T. J.; Caspar, J. V. *Chem. Rev.* **1985**, *85*, 187.
(70) Allen, D. M.; Cox, A.; Kemp, T. J.; Sultana, Q.; Pitts, R. B. *J. Chem. Soc., Dalton Trans.* **1976**, 1189.
(71) Van de Graaf, T.; Hofstra, R. M. J.; Schilder, P. G. M.; Rijkhoff, M.; Stufkens, D. J.; Van de Linden, J. G. M. *Organometallics* **1991**, *10*, 3668.

DOI: 10.1021/acs.inorgchem.5b00752
Inorg. Chem. 2015, 54, 6821−6828